Hysteresis enhancement on a hybrid Dy(III) Single Molecule Magnet/iron oxide nanoparticle system

Cite:
***Inorg. Chem. Front.*, 2019, DOI: 10.1039/C8QI01346B.**

Lidia Rosado Piquer,[a,b] Mariona Escoda-Torroella[a,b] Marisol Ledezma Gairaud,[c,d] Saul Carneros,[b] Niéli Daffé,[e] Michał Studniarek,[e] Jan Dreiser,[e] Wolfgang Wernsdorfer[f,g] and E. Carolina Sañudo [a,b,*]

In this paper we report the synthesis and characterization of hybrid molecular-inorganic systems composed of superparamagnetic iron oxide nanoparticles coated with a shell of oleic acid (NP) and $(Pr_2NH_2)_5[Dy_{12}(OH)_{16}(SALO)_4(SALOH)_8(NO_3)_8(H_2O)_{0.5}]NO_3$ (Dy_{12}) single-molecule magnets. The hybrid NP-Dy_{12} system presents an enhancement of the magnetization hysteresis with respect to the isolated components while retaining the morphological characteristics of the parent NPs.

Introduction

The rapid growth in high-speed computers and ultra high-density magnetic storage devices has stimulated high interest on the development of nanoscale magnetic materials.[1,2,3,4] Spintronics is now one of the most active areas of nanotechnology and in particular nanomagnetism. In molecular spintronics the aim is to combine spintronics with the possibilities offered by molecular systems such as single molecule magnets (SMMs)[5] that can exhibit the same properties of ferromagnetic materials[6] at the molecular level.[7,8] The efforts in preparing high performing SMMs have been focused in increasing spin[9–11] or anisotropy, with the latter being a more successful approach. Increasing anisotropy has been attempted by preparing heterometallic 3d-4f SMMs[12] or pure 4f SMMs,[13] which in most cases have not outperformed the archetypical SMM, Mn_{12}-Ac.[14,15] Very recently the goal has shifted to reaching the axial limit in linear Dy(III) complexes to achieve better SMMs.[16,17] Following this strategy, Layfield reported a dysprosocenium complex that displays record effective barrier and hysteresis up to 80 K,[18,19] Long *et al* reported a magnetostructural correlation for Dy metallocenes[20] and Reta and Chilton showed that vibrational phonon coupling had an important role in the energy barrier for magnetization reversal.[21]

The technologies of the future will require not only miniaturization but also low energy costs, and the use of one or several SMM molecules in functional devices implementing molecular spintronics would represent a giant step. The control and understanding of the intrinsic properties of the isolated SMM molecule on the surface and the interaction between the molecules and the surface is a key point. In the last decades several research groups worldwide have been dedicated to the study of surface deposition of molecular systems and their characterization. We have deposited nanomagnets and luminescent complexes on mica and HOPG (highly oriented crystalline pyrolytic graphite).[22,23] Most of the efforts have been devoted to the deposition of SMMs, such as those reported by Sessoli *et al.* on Mn_{12} and Fe_4 on surfaces of Au(111) or HOPG.[24–26] Carretta and Winpenny have deposited the Cr_7Ni nanomagnets on Au(111) with spectacular results.[27,28] Veciana,[29] Dreiser[30,31] and Ruben[32–34] have published excellent examples of the use of mononuclear $Tb(Pc)_2$ SMMs on surfaces or on carbon nanotubes. The transition metal-pthalocyanine complexes have been widely studied on magnetic surfaces, showing strong ferromagnetic coupling to the substrate that can be tuned by intercalation of a graphene layer between nanomagnet and substrate.[35] Gambardella and co-workers showed in 2011 how for the terbium pthalocyanine SMM $Tb(Pc)_2$ on Ni the SMM is coupled to the substrate but it behaves as a separate magnetic unit.[36] In 2016 Dreiser and Ruben demonstrated that an oxide thin film between the SMM and the substrate allows to observe the SMM's properties such as hysteresis.[30] These two last results show how a layer between molecule and substrate might play a really important role for the design of spintronic devices. This is further supported by the fact that the molecular properties can be affected by covalent grafting as shown by Murugesu in 2013: the dynamic properties of a Dy SMM were altered by coordination to Au nanoparticles, thus showing that covalent grafting of SMMs could greatly affect their properties[37] without apparently changing the substrate properties.

Iron oxide has been proposed as a good substrate to explore the interaction between an SMM and a magnetic substrate.[38] In particular, we have been interested in the use of iron oxide nanoparticles with a layer of an organic surfactant as substrate for SMMs.[39,40] Iron oxide nanoparticles of 10-20 nm are superparamagnetic and easy to fabricate[41] and they can perform many technological functions, such as being information storage units, sensors, contrast agents for imaging,[42,43] therapeutic agents[44,45] or drug carriers.[46] In most cases, a core-shell functionalization[47,48] is necessary to fine-tune the properties of the NP for the desired function. This is done most of the times using an inorganic shell with different magnetic properties from the iron oxide (magnetite in most cases) core.[49–51,52–54] Other strategies to prepare stable and well-defined nanomaterials based on star-like block copolymers as nanoreactors are also possible, with magnetic or plasmonic NP.[55–58] There have been few reports of iron oxide NP decorated or functionalized with SMMs or molecular magnets. In our two previous papers we showed that the SMMs grafted onto magnetite NP can retain their magnetic properties in the hybrid system.[39,40] Zoppellaro and co-workers showed how the local magnetic field of the NP can be used to change the properties of a softer magnetic shell, in which they embedded iron oxide NPs.[59] The effect however can go both ways, since the shell can also affect the properties of the core material. In 2015 Prado and coworkers demonstrated that the nanoparticle properties can be altered by surface modification with a paramagnetic system: a hysteresis enhancement was observed for Fe_2O_3 NP

with Co(II) paramagnetic complexes covalently bound to the surface.[60]

In this paper we report a hybrid molecular/inorganic system based on a dodecanuclear Dy(III) SMM and iron oxide NPs. We show how the decoration of monodisperse, superparamagnetic iron oxide NPs with the Dy(III) SMM Dy_{12} results in an enhancement of the magnetization vs. field hysteresis loop, which is observed at temperatures as high as 30 K.

Experimental

All the chemicals and solvents were purchased from commercial sources and used as received. Microwave assisted reactions were performed in a CEM Discover microwave reactor. SALOH stands for monodeprotonated 3,5-di-tert-butylsalicylic acid ($C_{15}H_{21}O_3^-$), while SALO for the deprotonated form ($C_{15}H_{20}O_3^{2-}$), Pr_2NH_2 stands for protonated dipropylamine.

$(Pr_2NH_2)_5[Dy_{12}(OH)_{16}(SALO)_4(SALOH)_8(NO_3)_8(H_2O)_{0.5}]NO_3\cdot 8(MeCN)\cdot 3.25(H_2O)\cdot(C_5H_{14}NO)NO_3$ (Dy_{12})

$Dy(NO_3)_3\cdot xH_2O$ (0.42 mmol, 0.147 g) and 3,5-di-tert-butylsalicylic acid (0.105 g, 0.42 mmol) were solved in 5 mL of MeCN. Then, 1-dimethylamino-2-propanol (51 µL, 0.42 mmol) and dipropylamine (58 µL, 0.42 mmol) were added leading to a colourless solution. The mixture was treated at the microwave at 140°C applying a power of 250 W during 5 minutes. The beige pale solution was cooled down to room temperature. Crystals were obtained by slow evaporation after 9 days. Dy_{12} was characterized using single crystal X-Ray Diffraction. Yield: 0.023 g (10%). Calculated Elemental Analysis for $(Pr_2NH_2)_5[Dy_{12}(OH)_{16}(SALO)_4(SALOH)_8(NO_3)_8(H_2O)_{0.5}]NO_3\cdot 3.25(H_2O)\cdot(C_5H_{14}NO)NO_3$: C, 39.50%; H, 5.64%; N, 3.43%. Found Elemental Analysis: C, 39.14%; H, 5.71%; N, 3.48%. IR data (KBr, cm^{-1}): 3434 (m, b), 3077 (w, b), 2958 (s), 2909 (w), 2870 (w), 1617 (m), 1551 (s), 1464 (w), 1446 (s), 1385 (s), 1365 (w), 1300 (w), 1245 (m), 1202 (m), 1151 (w), 1123 (w), 1026 (w), 817 (m), 744 (w), 723 (w); where strong (s), medium (m), weak (w), broad (b).

Iron oxide nanoparticles (NP)

The synthesis of iron oxide nanoparticles was carried out by modification of a published procedure [41]. Iron oleate (2.78 g, 3 mmol), oleic acid (0.96 mL, 3 mmol) and eicosane (10 mL) were mixed in a three neck round-bottom reaction flask and heated to 60 °C, to melt the solvent. Then the reaction mixture was heated to 366 °C, with a heating rate of 3.3 °C/min under stirring and kept refluxing for 10 min and then cooled down to 50 °C. To precipitate the NPs a mixture of 40 mL of acetone and 10 mL of hexane was added to the reaction flask. The NP were separated by centrifugation and washed with the acetone/hexane (4:1) mixture three times. Two different experiments yielded NP of 10.4 and 13.3 nm.

Preparation of hybrid NP-Dy_{12} system

20 mg of precipitate NPs were shaken with 2 mg of Dy_{12} in chloroform for 72 h. The decorated nanoparticles were magnetically separated and washed several times to avoid contamination with non-attached SMMs. The presence of Dy_{12} on the hybrid system was confirmed by the peaks of Dy on EDX (from TEM images) and XPS.

Characterization techniques. Infrared spectra were collected on a KBr pellet on an AVATAR 330 FT-IR at Departament de Química Inorgànica i Orgànica, Secció de Química Inorgànica, Universitat de Barcelona. The ^{1}H-NMR measurements were performed at the NMR Service of CCiT-UB on a Varian Unity 400 MHz. Elemental analysis was performed at Servei de Microanàlisi in CSIC (Consell Superior d'Investigacions Científiques). Single-crystal X-Ray diffraction were recorded on a Bruker APEXII SMART diffractometer using Molybdenum Kα microfocus (λ=0.71073 Å) as a radiation source belonging to GMMF. The structure was resolved by direct methods (SHELXS97) and refined in F2 (SHELX-97). Crystallographic file for Dy_{12} can be downloaded free of charge at the Cambridge Structural Datacentre (CCDC 1879195, http://www.ccdc.cam.ac.uk/). Magnetic measurements were performed at the Unitat de Mesures Magnètiques of the CCiT-University of Barcelona on a Quantum Design MPMS XL superconducting quantum interference device (SQUID) magnetometer equipped with a 5 T magnet. Diamagnetic corrections for the sample holder and for the sample using Pascal's constants were applied.

TEM: Specimens were analyzed using a JEOL JEM-2100 LaB6 transmission electron microscope with energy dispersed analysis of X-rays (EDX), operating at 200 kV. The spectrometer is an Oxford Instruments INCA x-sight, with Si (Li) detector, acquisition was accomplished using the INCA Microanalysis Suite version 4.09 software. Images were recorded with Gatan CCD Camera Orius SC1000 and Digital Micrograph v.1.82.80 software.

X-ray absorption spectroscopy (XAS) and X-ray magnetic circular dichroism (XMCD): The X-ray absorption measurements were performed at the X-Treme beam line[61] at the Swiss Light Source, Paul Scherrer Institut, Switzerland. Spectra were taken on a powder sample pressed into indium foil in total electron yield (TEY) mode. The X-ray beam direction and the magnetic field axis were parallel to each other, and the spot size at the sample was approximately 1 mm^2. The degree of circular polarization was 99.5 %. The spectra were normalized to the photon flux by simultaneously recording the TEY on a gold mesh, located before the measurement station. Spectra at remanence were obtained after applying a field of 6.8 T and then ramping down the field to 0.0 T.

Results and discussion

Usually high-nuclearity compounds have been synthesized via the "serendipitous self-assembly" approach.[1,62] Nevertheless, controlled synthesis[63] and microwave-assisted synthesis applied to coordination chemistry have also provided interesting results.[64,65] The microwave reactor offers a unique environment of high temperature and high pressure, generated by the super-heating of the reagents/solvent molecules with dipolar moment by the microwave radiation.[66,67] This results in shorter reaction times and in an enhancement of the reproducibility of the reactions. The microwave assisted reaction of hydrated $Dy(NO_3)_3$ with a salycilic acid derivative (3,5-ditertbutyl-2-hydroxy-benzoic acid, $SALOH_2$) in MeCN in

the presence of the weak base dipropylamine produces a dodecanuclear Dy(III) coordination complex, Dy_{12}. The complex co-crystallizes with the nitrate salt of protonated dimethylaminopropanol. If the dimethylaminopropanol was not part of the reaction mixture all our attempts failed to produce Dy_{12} in a crystalline form. Both in the microwave reactor or on normal benchtop conditions, precipitates were obtained the IR analysis of which showed similarities with Dy_{12}, but no single-crystals were obtained. This fact has been previously observed in similar reaction systems.[22,64] In this case, it could be attributed to the co-crystallization observed. The Dy_{12} molecules are very large and for efficient packing smaller molecules like dimethylaminopropanol are needed to fill the accessible voids (see the next section for more information). The reaction can be performed in regular benchtop conditions (stirring at room temperature) and a precipitate is obtained. The IR and magnetic properties of these precipitates confirms that they are indeed Dy_{12}. When the organic base is changed to triethylamine, a similar Dy_{12} complex is obtained, but other bases like pyridine do not produce Dy_{12} complexes.

Description of crystal structure

Crystallographic and data collection parameters for Dy_{12} are shown in Table 1. Crystal structural analysis reveals that Dy_{12} crystallizes in a triclinic system with the space group P-1. The metal-oxo core is composed by four $[Dy_4(\mu_3\text{-}OH)_4]^{8+}$ cubanes sharing two of the four dysprosium vertexes (Figure 1).

Table 1. Crystallographic and data collection parameters for Dy_{12} at 100K. R_1 = 0.0586 and wR = 0.1538.

Crystal system	Triclinic	α/°	105.294(2)
Space group	P-1	β/°	99.649(2)
a/Å	20.9834(10)	γ/°	98.715(2)
b/Å	22.3764(11)	Volume/Å-3	15739.6(13)
c/Å	36.0227(16)	Z	2

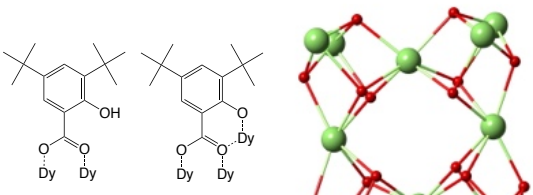

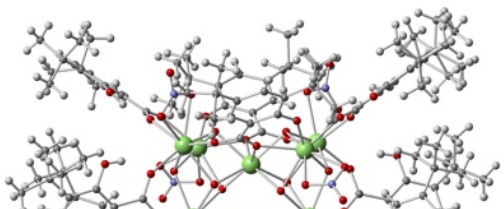

Figure 1. Crystal structure of Dy_{12}, showing the metal-oxide core and the whole structure, as a ball-and-stick representation and the different coordination modes of SALO and SALOH ligands. Carbon: grey; hydrogen: light grey; oxygen: red, nitrogen: light blue; dysprosium: green.

Each cubane is composed by four dysprosium(III) ions and four bridging μ_3-OH groups forming a distorted cubane $[Dy_4(\mu_3\text{-}OH)_4]^{8+}$. The Dy–O–Dy angles range from 90.9(1)° to 111.1(1)°. The core is surrounded by twelve SALOH ligands. Four are bridging two Dy ions in coordination mode I of Figure 1. The other four are bridging three Dy(III) ion in coordination mode II. These SALO ligands are coordinated to two Dy ions of different cubanes and to one in the shared vertex. The remaining four SALOH ligands are capping the $[Dy_4(\mu_3\text{-}OH)_4]^{8+}$ cubanes in coordination mode I. To complete their coordination sphere Dy(III) ions are coordinated to a bidentate nitrato ligand. All the Dy(III) ions are octacoordinated except one that is enneacoordinated in 50% of the molecules due to the coordination of a water molecule. Five protonated dipropylamine cations act as counterions and in the cavity formed by the SALO ligands there sit a nitrate and water molecule disordered over two positions. The nitrate salt of the protonated 1-dimethylamino-2-propanol co-crystallizes with the complex. The crystal structure shows large solvent accessible voids were additional severely disordered solvent molecules may sit. Dy_{12} is a new structural type for molecular Dy(III) complexes, however a MOF with structurally similar Na_2Dy_{12} nodes has been reported by Yi Xia Ren and co-workers.[68]

Magnetic properties of Dy_{12}

The temperature dependence of magnetic susceptibility of Dy_{12} was measured in the temperature range of 2.0 to 300 K with applied magnetic fields of 198 and 3000 Oe. As shown in Figure 2, the experimental χT value of 169 $cm^3 \cdot K \cdot mol^{-1}$ at 300 K for Dy_{12} is in agreement with the expected value of 170 $cm^3 \cdot K \cdot mol^{-1}$ for twelve uncoupled Dy(III) ions (S = 5/2, $^6H_{15/2}$, g = 4/3). Upon cooling the value gradually decreases down to 50 K, below this

temperature the χT product sharply decreases to reach 99 $cm^3 \cdot K \cdot mol^{-1}$ due to the progressive depopulation of excited M_J sublevels. The Dy–O–Dy angles of Dy_{12} are similar to those of reported Dy_4 cubane-like compounds with weak ferromagnetic coupling that exhibit slow magnetic relaxation.[69,70]

a)

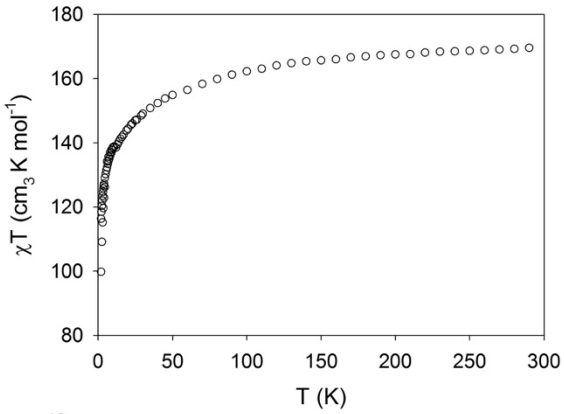

b)

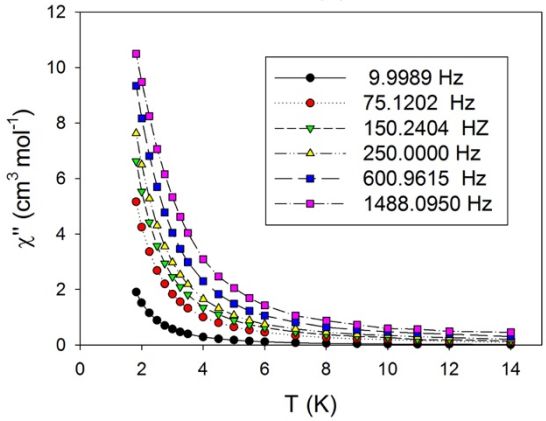

Figure 2. A) Magnetic susceptibility data as χT vs T plot for Dy_{12} at dc field of 0.5 T. B) Out-of-phase (χ'') magnetic susceptibility vs. T for Dy_{12} at the indicated frequencies for the oscillating field (solid lines are guides for the eye).

The magnetization vs field at 2 K at first increases rapidly and then slowly without reaching full saturation at 5 T (Figure S1). The maximum value for M is 65 μ_B for Dy_{12}. This value is lower than the expected saturation value of 120 μ_B for twelve free dysprosium ions, which along with the lack of saturation on the M vs. H data at 2 K suggests the presence of a combination of weak magnetic exchange and magnetic anisotropy in Dy_{12}.[71,72] The relaxation dynamics of magnetization were investigated using Alternate Current (AC) susceptibility measurements.

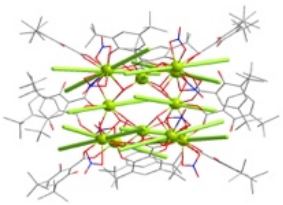

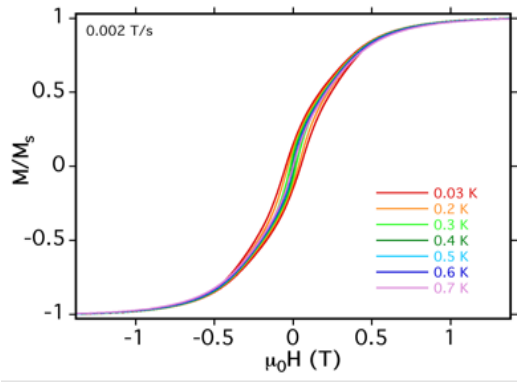

Figure 3. Anisotropy axes on each Dy(III) ion calculated with Magellan, (top) view along z, (bottom) view on the xy plane. Magnetization vs. field hysteresis for Dy_{12} measured using a microsquid as a function of scan rate and temperature. At 0.03K Hc = 425 Oe.

Figure 2 shows the out-of-phase (χ'') signal vs T for Dy_{12} at various frequencies of the oscillating ac field. Only the tail of an out-of-phase peak is observed. Molecular anisotropy can be affected by the local tensor of anisotropy on each Dy ion and their relative orientations leading to slow relaxation of the magnetization, although the magnetic interactions are expected to be very weak. These can be modelled with Magellan.[73] The program relies on an electrostatic model and a doublet ground state for Dy(III) quantized along the anisotropy axis with m_J=±15/2. Figure 3 shows the anisotropy axes for each Dy(III) as calculated by Magellan. Not all twelve anisotropy axes align parallel, but they are not completely perpendicular, thus they provide the Dy_{12} with some axial anisotropy. This is in agreement with Dy_{12} having a small energy barrier for magnetization relaxation, as obtained from ac data. The out-of-phase ac susceptibility data was fitted using a Debye model between 1.8 and 3.2 K. The relaxation times obtained for the fitting were used to extract an effective energy barrier using Arrhenius model: U_{eff} = 5.75 K and τ_o = 1.827e-7 s^{-1} with α values between 0.46 and 0.51. The large values of α indicate a wide distribution of relaxation processes, as expected due to the crystallographic disorder (see Supplementary Information, Table S1 for fitting parameters and Arrhenius plot). Dy_{12} did not display hysteresis of the magnetization down to 2 K, so the hysteresis at lower temperatures were studied using a microsquid. Magnetization vs. field hysteresis loops were collected as a function of the scan rate and as a function of temperature. The opening of a narrow hysteresis loop below 1 K can be observed, as shown in Figure 3, with broad features. A clear dependence on the field scan rate is observed, as expected for SMMs. High nuclearity molecules often present broad steps in their hysteresis loops due to the existence of several pathways for magnetic relaxation, in agreement with the large alfa values obtained from the Debye model.[74,75]

Preparation of hybrid molecular/inorganic systems

Iron oxide NP can be prepared in monodisperse form and can be functionalized with surfactants such as dopamine, oleylamine or oleic acid. In this way, the nature of the exposed

surface for interaction with a molecule can be tuned. Given the hydrophobic nature of our complex Dy_{12}, with exposed tert-butyl groups, oleic acid was chosen as surfactant to promote a large number of weak Van der Waals interactions between the aliphatic groups.[76] The nanoparticles were prepared following reported procedures by the thermal decomposition method. By this controlled synthesis one can obtain monodisperse, crystalline iron oxide NP of diameters between 10-20 nm. Two experiments provided NPs of 10.4 nm diameter with a relative standard deviation (RSD) of 6.8% and NPs of 13.1 nm diameter with a RSD of 5.3%, in agreement with the published procedure.[41,77]

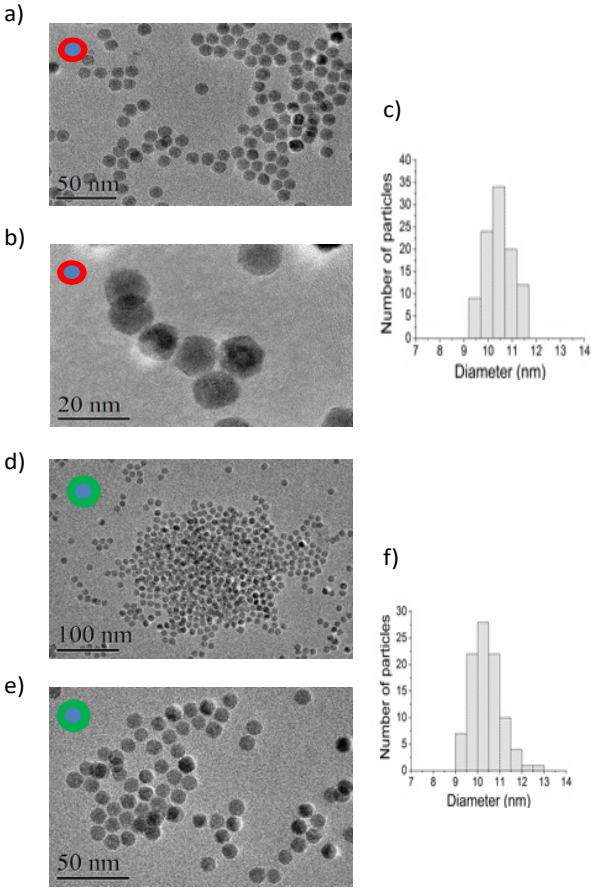

Figure 4. Transmission Electron Microscope images of oleic acid coated NPs (A and B) and the hybrid material NP-Dy_{12} (D and E). The cartoon is a schematic representation of the core/shell system where shell = oleate (red) or oleate/Dy_{12} (green) and core = iron oxide NP (blue). Histograms for the sample of oleic acid coated NP (C) and the hybrid material NP-Dy_{12} (F).

The obtained iron oxide nanoparticles were characterized by TEM and SQUID. The NP were crystalline, and diffraction pattern obtained at the TEM coincide with magnetite, Fe_3O_4. The iron oxide NP are coated with a self-assembled monolayer of oleate. In order to prepare the core-shell hybrid NP-Dy_{12} material a sample of NP and of Dy_{12} were dissolved in $CHCl_3$ and mechanically shaken at room temperature for 72 h. After this time, the NP-Dy_{12} were separated using a hard magnet. The black solid was dispersed and washed with $CHCl_3$ several times, in order to remove Dy_{12} not attached to the NP. The hybrid material was characterized by TEM and EDX, TEM images are shown in Figure 4. The core-shell hybrid material NP-Dy_{12} is formed by fairly monodisperse and crystalline iron oxide NP coated by an oleic acid/Dy_{12} shell, Figure 4 shows a cartoon of the material with the TEM images. The NP-Dy_{12} have diameters of 10.4 nm with a RSD of 5.4% (Figure 4) and 13.3 nm with a RSD of 10.5% (Supplementary material). The Energy-Dispersive X-Ray spectroscopy (EDX, Figure S4) showed the presence of Dy on the nanoparticles. The iron oxide NP as observed by TEM suffer no change in size, shape or aggregation when they are decorated with Dy_{12} SMMs. In contrast, a blank sample of NP that underwent the functionalization process without the addition of Dy_{12} SMM showed greater size changes and a much more noticeable aggregation as observed by TEM (Figure S8). The average distance between iron oxide NP cores in oleic acid coated NP and NP-Dy_{12} is approximately the same, about 2-3 nm. This fact could imply that Dy_{12} SMMs are embedded or wedged into the oleic acid shell, even replacing some of the oleic acid. Molecules with the SALO ligand have a tendency to have hydrophobic pockets where aliphatic chains fit very well. We have seen this before in coordination complexes that contain the SALO ligand[63] and this is again observed in the crystal packing of Dy_{12}. This kind of CH--HC Van der Waals interactions are important, even though weak, in particular for tert-butyl groups[76] and can be relevant in many instances of self-organization, in example in complex molecule deposition,[78] or in substituted C_{60} molecules that form dynamic crystalline frameworks held together by these kind of interactions, also called 'sticky fingers'.[79] An approximation can be done to calculate the number of molecules surrounding each nanoparticle, assuming a model system with only one layer of molecules on each NP. The dimensions of each Dy_{12} complex can be extracted from the crystal structure. In the unit cell, two molecules pack in a volume of 15.73 nm^3, so each Dy_{12} has approximate dimensions of 2x2x1.5 nm^3. Assuming that the NPs are spherical and a radius of 5 nm each NP has a surface of 314 nm^2 that is covered by oleic acid. A number between 50 and 150 molecules of Dy_{12} could be grafted onto the NP in one single layer or embedded on the oleic acid shell. XPS analysis of the D_{12}-NP sample showed small peaks corresponding to Dy (Figure S5). Thermogravimetric analysis (Figures S5 and S6) shows different profiles of organic matter loss up to 500°C for oleate-NP (9.2 and 6.2 % weight loss for 10.4 nm and 13.1 nm NPs respectively) and Dy_{12}-SMM hybrid system (11.4 and 7.4 % weight loss for 10.4 nm and 13.1 nm iron oxide core NPs respectively). The values obtained agree with an incomplete coverage of the surface of oleate-NP with Dy_{12} SMMs.

Magnetic characterization of hybrid SMM-NP systems

The oleic acid covered NP are magnetic at room temperature and the hybrid system D_{12}-NP retains this property. Ac magnetic susceptibility data and magnetization vs. field hysteresis data were collected. Data are shown in Figure 5. These nanoparticles are superparamagnetic. At 2 K the iron oxide NP are blocked and present a small coercive field Hc = 50 Oe (10.4 nm NPs, Figure 5B) and 375 Oe (13.1 nm NPs, Supplementary material). The saturation value per gram of material (including the oleic acid) for the magnetization Ms at 5 T is 50.14 $emu \cdot g^{-1}$. The hybrid

systems NP-Dy_{12} are also magnetic at room temperature and can thus be separated using a hard magnet.

AC measurements were done on the hybrid NP-Dy_{12} systems to determine the blocking temperature of the superparamagnetic nanoparticles and are shown in Figure 6 for 10.4 nm NPs The hybrid system presents a small shift in the ac magnetic susceptibility blocking temperature: for NP-Dy_{12} the maximum shifts to 130 K at 1000 Hz. In addition, more pronounced frequency dependence is observed for NP-Dy_{12} than for the untreated NP and a small feature that was not present in the out-of-phase ac magnetic susceptibility of the NP appears around 30-50 K for NP-Dy_{12}. Similar results are obtained for NP-Dy_{12} with 13.1 nm parent NPs (see Supplementary material). This feature cannot be readily assigned to Dy_{12}. The NP-Dy_{12} present an enhancement of the hysteresis of the magnetization *vs.* field with respect to the isolated NP or Dy_{12} at the same temperatures.

a)

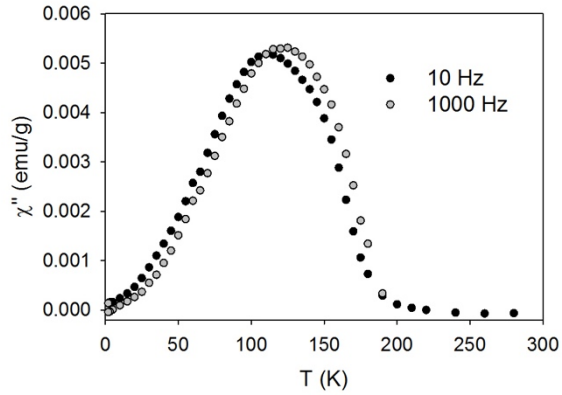

b)

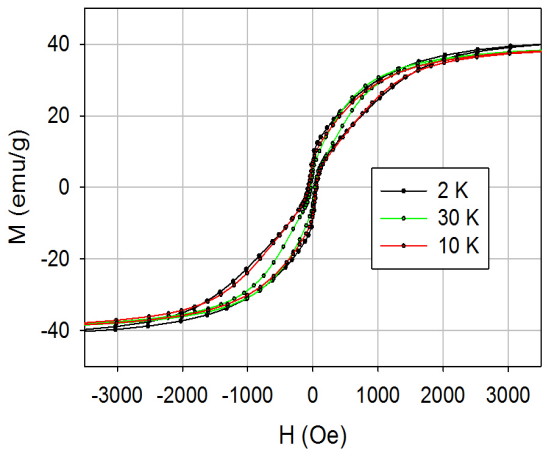

Figure 5. A: Out-of-phase AC magnetic susceptibility data for iron oxide nanoparticles with oleic acid surfactant at two frequencies (10 Hz and 1000 Hz; no applied dc field). B: magnetization vs. field hysteresis for the oleic acid covered iron oxide NP (10.4 nm) at 2 K.

The data are shown for 10.4 nm parent NP in Figure 6. For NP-Dy_{12} at 2 K the saturation magnetization per gram of material (including oleic acid and Dy_{12} SMM) at 5 T Ms is 55.48 emu·g^{-1}, larger than that of the NP before decoration with Dy_{12}. The NP-Dy_{12} hybrid system at 2K has a Hc of 487 Oe, nearly ten times the coercive field of the oleic acid coated iron oxide NP at the same temperature for NP of 10.4 nm. Larger iron oxide NP of 13.1 nm were also functionalized with Dy_{12} SMMs, an enhancement of the hysteresis was also observed but the effect was less pronounced: the coercive field at 2 K for the NP-Dy_{12} system was 5.4 times larger than that of the parent 13.1 nm NPs. A sample of NP that underwent the functionalization treatment without SMMs showed clearly extensive aggregation in TEM images and thus the observed magnetic properties can be attributed to this aggregation. Hysteresis loops were collected for the hybrid system at 8 K, 30 K, 100 K and 200 K. The hybrid system NP-Dy_{12} (10.4 nm) still presents hysteresis of the magnetization with Hc = 100 Oe up to 30 K and NP-Dy_{12} (13.4 nm) shows Hc = 700 Oe at 100 K. At 200 K, above the blocking temperature of the iron oxide NP, the hybrid system does not present hysteresis, as expected. The magnetization vs. field hysteresis loops for NP-Dy_{12} at 2K and 8 K show a step that can be attributed to the addition of the hysteresis loops of the NP material and the hysteresis loop of the SMMs Dy_{12}.[80]

a)

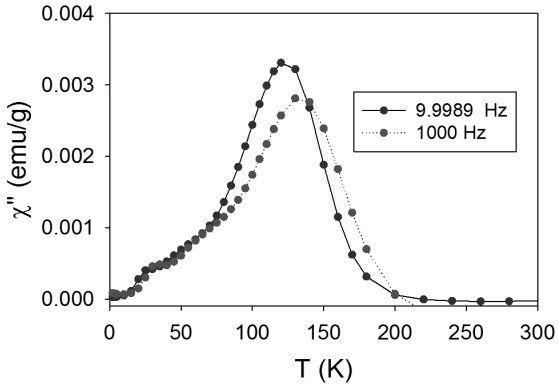

b)

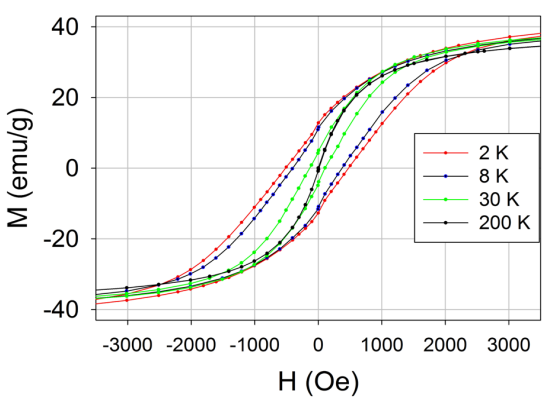

Figure 6. A) Out-of-phase AC magnetic susceptibility plot for NP-Dy_{12} (10.4 nm) and B) magnetization vs. field hysteresis for the hybrid system NP-Dy_{12} (10.4 nm) at various temperatures.

The ZFC hysteresis loops for NP-Dy_{12} show a small exchange bias field of -28 Oe (10.4 nm) at 2 K. Hysteresis cycles were measured at different field cool magnetic fields. They all showed an exchange bias fields (HE) that shifts to more negative values as the FC field is increased below 1T (see Supplementary Material, Figure S2) and at fields above 1 T HE shifts to more positive values. Similar results were observed for the larger NP-Dy_{12} system. This kind of horizontal shift in the hysteresis loops is usually attributed to antiferromagnetic coupling.[36,49,81] Exchange bias has been observed in core-shell NP,[49] in coupled

aggregates of SMMs[82,83] or on SMMs coupled to a magnetic surface[33,84] additionally to the seminal studies on biasing on heteromagnetic multilayers.[81,85,86] To ascertain the origin of the enhanced hysteresis in NP-Dy_{12} X-ray magnetic circular dichroism (XMCD) data were collected at the Fe $L_{2,3}$ and Dy $M_{4,5}$ edges, which reveal the element specific contributions to the magnetic properties. The strength of the XMCD signal is known to be proportional to the total, spin and orbital, magnetic moment localized in the Fe 3d and the Dy 4f shells, respectively. The XAS and XMCD data recorded at 2 K on the hybrid NP-Dy_{12} are shown in Figure 7. The absence of a remanent magnetization on the Dy ions shows that they do not contribute directly to the remanence enhancement with respect to the pristine NPs. Thus, the hysteresis enhancement is due to the iron oxide NP of the hybrid system. Clearly, a synergic effect between the anisotropic Dy_{12} layer and the relaxation dynamics of iron oxide leads to the observed hysteresis enhancement. Furthermore, the lack of remanence XMCD signal at the Dy edge is indicative that the coupling between Dy_{12} and iron oxide NP is very weak and not observable at the temperature of the measurement.

A spin-canting phenomena on the surface of the magnetite NP similar to the effect of ultrathin shells observed by Moon et al[53] or enhanced interparticle coupling[87] through the paramagnetic layer of Dy_{12}, as observed for multilayer systems by Magnus et al[88] could be responsible for the hysteresis enhancement, however this is not supported by the magnetization data.

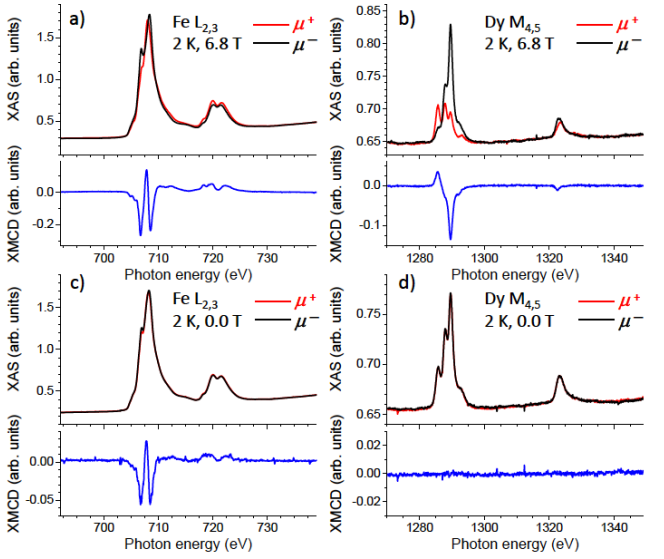

Figure 7. XAS and XMCD recorded on a powder sample of NP-Dy_{12} at the (a,c) Fe $L_{2,3}$ and (b,d) Dy $M_{4,5}$ edges at 2 K in field and at remanence as indicated in the plots.

The ratio between remanence magnetization and saturation magnetization Mrem/Msat for the iron oxide NP is 0.20 while for the hybrid system NP-Dy_{12} it is 0.24 for 10.4 nm NP. The values are similar for larger NP and NP-Dy_{12} and indicate antiferromagnetic inter-NP interactions that are similar in both systems, before and after decoration with Dy_{12} SMM. A similar enhancement of the magnetic properties of the iron oxide NPs has been observed by Prado *et al.* by coordination of a Co(II) coordination complex to Fe_2O_3 NPs.[60] They propose that covalent linking of the two species through oxo-bridges and the resulting magnetic interaction are key for the observed enhancement of the magnetic properties. In the reported hybrid system the through-space interaction between Dy_{12} and the iron oxide via the oleic acid monolayer results in a significant enhancement of the magnetic properties of the NP without affecting morphology, shape, size or aggregation of the functionalized NP. The large magnetic moment of Dy_{12} is directly related to the hysteresis enhancement observed since other hybrid systems with Dy[40] or 3d-4f[39] complexes previously reported by us did not display such manifest hysteresis enhancement. Furthermore, the effect observed is directly related to the surface/volume ratio of the parent NP: the enhancement is more important for smaller NP. For a surface/volume ratio of 19% the coercive field is 10 times larger upon functionalization with Dy_{12} while for a surface/volume ratio of 15% the coercive field is just 5 times larger for the hybrid system.

Conclusion

Hybrid molecular/inorganic NP-Dy_{12} systems have been prepared with Dy_{12} SMMs and iron oxide NP. In this system Dy_{12} is separated from the magnetic iron oxide substrate by an oleate layer and Dy_{12} SMMs are isolated from each other. The hybrid system displays enhanced magnetization hysteresis up to 100 K, depending on the size of the parent NP. The magnitude of the effect is size-dependent and thus directly related to the surface/volume ratio of the parent NP. Applications such as information storage in core-shell NPs are proposed but are hampered by overall morphology deterioration caused by the usual means of growing the shell from the core. Hybrid SMM-NP systems are promising, since they can overcome some of the problems core-shell NP present like morphology deterioration and aggregation but there are still many issues to be addressed such as the possibility of self-assembly of SMM-NP, robustness or thermal stability. Furthermore, implications to molecular spintronics are important since surface modification of a substrate with SMMs can have important effects even if the SMM is not strongly coupled to the substrate. To avoid this strong coupling of the SMM to the surface, an intermediate material is necessary, as we show here, a SAM of simple organic molecules can be used to this effect. In summary, here we show a post-synthetic approach to fine tuning the magnetic properties of iron oxide NP without affecting their morphological or structural properties (size and shape) with enhanced magnetic properties. This can open up new possibilities for application of such hybrid systems by taking advantage of the enhanced Hc and of the control on the SMM-NP system afforded by the wet chemical post-synthesis modification of the NP.

Conflicts of interest

There are no conflicts to declare.

Acknowledgements

ECS and LRP acknowledge the financial support from the Spanish Government, (Grant CTQ2015-68370-P). WW acknowledges the Agence Nationale de la Recherche (France) for project MolQuSpin, ANR-13-BS10. MLG acknowledges CELEQ and Universidad de Costa Rica (Costa Rica) for funding her visit to GMMF at the Universitat de Barcelona. This project was supported by the Swiss National Science Foundation (grant no. 200021_165774/1) and by the European Union's Horizon 2020 research and innovation programme under the Marie Skłodowska-Curie grant agreement no. 701647.

Notes and references

‡ Footnotes relating to the main text should appear here. These might include comments relevant to but not central to the matter under discussion, limited experimental and spectral data, and crystallographic data.

1 G. Aromí and E. K. Brechin, *Single-molecule mgnets and related phenomena*, Springer Berlin Heidelberg, Berlin, 2006.

2 a. L. Barra, a. Caneschi, a. Cornia, F. Fabrizi de Biani, D. Gatteschi, C. Sangregorio, R. Sessoli and L. Sorace, *J. Am. Chem. Soc.*, 1999, **121**, 5302–5310.

3 A. Dei and D. Gatteschi, *Angew. Chemie - Int. Ed.*, 2011, **50**, 11852–11858.

4 P. Zhang, Y. N. Guo and J. Tang, *Coord. Chem. Rev.*, 2013, **257**, 1728–1763.

5 E. Coronado and M. Yamashita, *Dalt. Trans.*, 2016, **80**, 1517.

6 S. V. Eliseeva and J.-C. G. Bünzli, *New J. Chem.*, 2011, **35**, 1165.

7 M. Soler, W. Wernsdorfer, K. Folting, M. Pink and G. Christou, *J. Am. Chem. Soc.*, 2004, **126**, 2156–2165.

8 E. C. Sañudo, M. Font-Bardia, X. Solans and R. H. Laye, *New J. Chem.*, 2011, **35**, 842–848.

9 E. K. Brechin, C. Boskovic, W. Wernsdorfer, J. Yoo, A. Yamaguchi, E. C. Sanudo, T. R. Concolino, A. L. Rheingold, H. Ishimoto, D. N. Hendrickson and G. Christou, *J. Am. Chem. Soc.*, 2002, **124**, 9710–9711.

10 A. M. Ako, I. J. Hewitt, V. Mereacre, R. Clérac, W. Wernsdorfer, C. E. Anson and A. K. Powell, *Angew. Chem. Int. Ed. Engl.*, 2006, **45**, 4926–4929.

11 A. M. Ako, S. Alam, S. Mameri, Y. Lan, M. Hibert, M. Stocker, P. Müller, C. E. Anson and A. K. Powell, 2012, 4131–4140.

12 L. Rosado Piquer and E. C. Sañudo, *Dalt. Trans.*, 2015, **44**, 8771–8780.

13 D. N. Woodruff, R. E. P. Winpenny and R. A. Layfield, *Chem. Rev.*, 2013, **113**, 5110–5148.

14 R. Bagai and G. Christou, *Chem. Soc. Rev.*, 2009, **38**, 1011–26.

15 R. Sessoli, H.-L. Tsai, A. R. Schake, S. Wang, J. B. Vincent, K. Folting, D. Gatteschi, G. Christou and D. N. Hendrickson, *J. Am. Chem. Soc.*, 1993, **115**, 1804–1816.

16 S. a Sulway, R. a Layfield, F. Tuna, W. Wernsdorfer and R. E. P. Winpenny, *Chem. Commun. (Camb).*, 2012, **48**, 1508–10.

17 S. Demir, M. D. Boshart, J. F. Corbey, D. H. Woen, M. I. Gonzalez, J. W. Ziller, K. R. Meihaus, J. R. Long and W. J. Evans, *Inorg. Chem.*, 2017, **56**, 15049–15056.

18 F. S. Guo, B. M. Day, Y. C. Chen, M. L. Tong, A. Mansikkamäki and R. A. Layfield, *Angew. Chemie - Int. Ed.*, 2017, **56**, 11445–11449.

19 F. Guo, B. M. Day, Y. Chen, M. Tong, A. Mansikkamäki and R. A. Layfield, *Science (80-.).*, 2018, **0652**, 10.1126/science.aav0652.

20 K. R. McClain, C. A. Gould, K. Chakarawet, S. Teat, T. J. Groshens, J. R. Long and B. G. Harvey, *Chem. Sci.*, 2019, DOI: 10.1039/C8SC03907K.

21 C. A. P. Goodwin, F. Ortu, D. Reta, N. F. Chilton and D. P. Mills, *Nature*, 2017, **548**, 439–442.

22 A. Pons-balagué, S. Piligkos, S. J. Teat, J. Sánchez Costa, M. Shiddiq, S. Hill, G. R. Castro, P. Ferrer-Escorihuela and E. C. Sañudo, *Chem. Eur. J.*, 2013, **19**, 9064–9071.

23 M. J. Heras-Ojea, D. R. Mañeru, L. Rosado, J. R. Zuazo, G. R. Castro, S. Tewary, G. Rajaraman, G. Aromí, E. Jiménez and E. C. Sañudo, *Chem. - A Eur. J.*, 2014, **20**, 10439–10445.

24 M. Mannini, F. Pineider, P. Sainctavit, C. Danieli, E. Otero, C. Sciancalepore, A. M. Talarico, M.-A. Arrio, A. Cornia, D. Gatteschi and R. Sessoli, *Nat. Mater.*, 2009, **8**, 194–197.

25 L. Malavolti, V. Lanzilotto, S. Ninova, L. Poggini, I. Cimatti, B. Cortigiani, L. Margheriti, D. Chiappe, E. Otero, P. Sainctavit, F. Totti, A. Cornia, M. Mannini and R. Sessoli, *Nano Lett.*, 2015, **15**, 535–541.

26 D. Gatteschi, A. Cornia, M. Mannini and R. Sessoli, *Inorg. Chem.*, 2009, **48**, 3408–3419.

27 V. Corradini, a Ghirri, E. Garlatti, R. Biagi, V. De Renzi, U. del Pennino, V. Bellini, S. Carretta, P. Santini, G. Timco, R. E. P. Winpenny and M. Affronte, *Adv. Funct. Mater.*, 2012, **22**, 3706–3713.

28 A. Ghirri, V. Corradini, V. Bellini, R. Biagi, U. del Pennino, V. De Renzi, J. C. Cezar, C. A. Muryn, G. A. Timco, R. E. P. Winpenny and M. Affronte, *ACS Nano*, 2011, **5**, 7090–9.

29 J. Gómez-Segura, I. Díez-Pérez, N. Ishikawa, M. Nakano, J. Veciana and D. Ruiz-Molina, *Chem. Commun. (Camb).*, 2006, 2866–2868.

30 C. Wäckerlin, F. Donati, A. Singha, R. Baltic, S. Rusponi, K. Diller, F. Patthey, M. Pivetta, Y. Lan, S. Klyatskaya, M. Ruben, H. Brune and J. Dreiser, *Adv. Mater.*, 2016, **28**, 5195–5199.

31 J. Dreiser, C. Wäckerlin, M. E. Ali, C. Piamonteze, F. Donati, A. Singha, K. S. Pedersen, S. Rusponi, J. Bendix, P. M. Oppeneer, T. A. Jung and H. Brune, *ACS Nano*, 2014, **8**, 4662–4671.

32 J. Schwöbel, Y. Fu, J. Brede, A. Dilullo, G. Hoffmann, S. Klyatskaya, M. Ruben and R. Wiesendanger, *Nat. Commun.*, 2012, **3**, 953.

33 A. L. Rizzini, C. Krull, T. Balashov, A. Mugarza, C. Nistor, F. Yakhou, V. Sessi, S. Klyatskaya, M. Ruben, S. Stepanow and P. Gambardella, *Nano Lett.*, 2012, 5703–5707.

34 M. Urdampilleta, S. Klyatskaya, J. -p. Cleuziou, M. Ruben and W. Wernsdorfer, *Nat. Mater.*, 2011, **10**, 502–506.

35 G. Avvisati, C. Cardoso, D. Varsano, A. Ferretti, P. Gargiani

and M. G. Betti, *Nano Lett.*, 2018, **18**, 2268–2273.
36 A. Lodi Rizzini, C. Krull, T. Balashov, J. J. Kavich, A. Mugarza, P. S. Miedema, P. K. Thakur, V. Sessi, S. Klyatskaya, M. Ruben, S. Stepanow and P. Gambardella, *Phys. Rev. Lett.*, 2011, **107**, 177205.
37 R. J. Holmberg, A. Hutchings, F. Habib, I. Korobkov, J. C. Scaiano and M. Murugesu, *Inorg. Chem.*, 2013, **52**, 14411–14418.
38 V. E. Campbell, M. Tonelli, I. Cimatti, J.-B. Moussy, L. Tortech, Y. J. Dappe, E. Rivière, R. Guillot, S. Delprat, R. Mattana, P. Seneor, P. Ohresser, F. Choueikani, E. Otero, F. Koprowiak, V. G. Chilkuri, N. Suaud, N. Guihéry, A. Galtayries, F. Miserque, M.-A. Arrio, P. Sainctavit and T. Mallah, *Nat. Commun.*, 2016, **7**, 13646.
39 L. Rosado Piquer, E. Jiménez, Y. Lan, W. Wernsdorfer, G. Aromi and E. C. Sañudo, *Inorg. Chem. Front.*, 2017, **4**, 595–603.
40 L. Rosado Piquer, R. Royo Sánchez, E. C. Sañudo and J. Echeverrerría, *Molecules*, 2018, **23**, 1441–1456.
41 L. M. Bronstein, X. Huang, J. Retrum, A. Schmucker, M. Pink, B. D. Stein and B. Dragnea, *Chem. Mater.*, 2007, **19**, 3624–3632.
42 L. H. Reddy, J. L. Arias, J. Nicolas and P. Couvreur, *Chem. Rev.*, 2012, **112**, 5818–5878.
43 M. Colombo, S. Carregal-Romero, M. F. Casula, L. Gutiérrez, M. P. Morales, I. B. Böhm, J. T. Heverhagen, D. Prosperi and W. J. Parak, *Chem. Soc. Rev.*, 2012, **41**, 4306.
44 R. Hergt, S. Dutz, R. Müller and M. Zeisberger, *J. Phys. Condens. Matter*, 2006, **18**, S2919–S2934.
45 A. Espinosa, R. Di Corato, J. Kolosnjaj-Tabi, P. Flaud, T. Pellegrino and C. Wilhelm, *ACS Nano*, 2016, acsnano.5b07249.
46 T. C. Johnstone, N. Kulak, E. M. Pridgen, O. C. Farokhzad, R. Langer and S. J. Lippard, *ACS Nano*, 2013, **7**, 5675–5683.
47 P. Guardia, B. Batlle-Brugal, A. G. Roca, O. Iglesias, M. P. Morales, C. J. Serna, A. Labarta and X. Batlle, *J. Magn. Magn. Mater.*, 2007, **316**, 756–759.
48 J. Salafranca, J. Gazquez, N. Pérez, A. Labarta, S. T. Pantelides, S. J. Pennycook, X. Batlle and M. Varela, *Nano Lett.*, 2012, **12**, 2499–2503.
49 M. Estrader, A. López-Ortega, S. Estradé, I. V. Golosovsky, G. Salazar-Alvarez, M. Vasilakaki, K. N. Trohidou, M. Varela, D. C. Stanley, M. Sinko, M. J. Pechan, D. J. Keavney, F. Peiró, S. Suriñach, M. D. Baró and J. Nogués, *Nat. Commun.*, 2013, **4**, 2960.
50 A. López-Ortega, M. Estrader, G. Salazar-Alvarez, A. G. Roca and J. Nogués, *Phys. Rep.*, 2015, **553**, 1–32.
51 a López-Ortega, M. Estrader, G. Salazar-Alvarez, S. Estradé, I. V Golosovsky, R. K. Dumas, D. J. Keavney, M. Vasilakaki, K. N. Trohidou, J. Sort, F. Peiró, S. Suriñach, M. D. Baró and J. Nogués, *Nanoscale*, 2012, **4**, 5138–47.
52 E. A. Kwizera, E. Chaffin, Y. Wang and X. Huang, *RSC Adv.*, 2017, **7**, 17137–17153.
53 S. H. Moon, S. H. Noh, J. H. Lee, T. H. Shin, Y. Lim and J. Cheon, *Nano Lett.*, 2017, **17**, 800–804.
54 Y. Prado, N. Dia, L. Lisnard, G. Rogez, F. Brisset, L. Catala and T. Mallah, *Chem. Commun.*, 2012, **48**, 11455.
55 Z. Lin, , DOI:10.1039/c8nr07115b.
56 C. Feng, X. Pang, Y. He, Y. Chen, G. Zhang and Z. Lin, , DOI:10.1039/c5py00765h.
57 Y. W. Harn, M. He, S. Zhang, G. Zhang and Z. Lin, , DOI:10.1021/jacs.7b04545.
58 C. S. Nanoparticles, D. Yang, X. Pang, Y. He, Y. Wang, G. Chen, W. Wang and Z. Lin, 2015, **100081**, 12091–12096.
59 G. Zoppellaro, J. Tuček, R. Herchel, K. Šafářová and R. Zbořil, *Inorg. Chem.*, 2013, **52**, 8144–8150.
60 Y. Prado, N. Daffé, A. Michel, T. Georgelin, N. Yaacoub, J. M. Grenèche, F. Choueikani, E. Otero, P. Ohresser, M. A. Arrio, C. Cartier-Dit-Moulin, P. Sainctavit, B. Fleury, V. Dupuis, L. Lisnard and J. Fresnais, *Nat. Commun.*, 2015, **6**, 10139.
61 C. Piamonteze, U. Flechsig, S. Rusponi, J. Dreiser, J. Heidler, M. Schmidt, R. Wetter, M. Calvi, T. Schmidt, H. Pruchova, J. Krempasky, C. Quitmann, H. Brune and F. Nolting, *J. Synchrotron Radiat.*, 2012, **19**, 661–674.
62 E. C. Sañudo, J. S. Uber, A. Pons Balagué, O. Roubeau and G. Aromí, *Inorg. Chem.*, 2012, **51**, 8441–8446.
63 M. Ledezma-Gairaud, L. Grangel, G. Arom??, T. Fujisawa, A. Yamaguchi, A. Sumiyama and E. C. Sa??udo, *Inorg. Chem.*, 2014, **53**, 5878–5880.
64 A. Pons-Balague, N. Ioanidis, W. Wernsdorfer, A. Yamaguchi and E. C. Sanudo, *Dalt. Trans.*, 2011, **40**, 11765–11769.
65 M. Ledezma-Gairaud, L. W. Pineda, G. Aromí and E. C. Sañudo, *Polyhedron*, 2013, **64**, 45–51.
66 A. Pons-Balagué, M. J. Heras Ojea, M. Ledezma-Gairaud, D. Reta Mañeru, S. J. Teat, J. Sánchez, G. Aromí and E. C. Sañudo, *Polyhedron*, 2013, **52**, 781–787.
67 B. L. Hayes, *Microwave Synthesis: Chemistry at the Speed of Light*, CEM Publishing, U.S.A., 2002.
68 Y. X. Ren, X. J. Zheng, L. C. Li, D. Q. Yuan, M. An and L. P. Jin, *Inorg. Chem.*, 2014, **53**, 12234–12236.
69 Y. Gao, G.-F. Xu, L. Zhao, J. Tang and Z. Liu, *Inorg. Chem.*, 2009, **48**, 11495–11497.
70 H. Ke, P. Gamez, L. Zhao, G. F. Xu, S. Xue and J. Tang, *Inorg. Chem.*, 2010, **49**, 7549–7557.
71 Y.-L. Miao, J.-L. Liu, J.-D. Leng, Z.-J. Lin and M.-L. Tong, *CrystEngComm*, 2011, **13**, 3345–3347.
72 S. Das, A. Dey, S. Biswas, E. Colacio and V. Chandrasekhar, *Inorg. Chem*, 2014, **53**, 3417–3426.
73 N. F. Chilton, D. Collison, E. J. L. McInnes, R. E. P. Winpenny and A. Soncini, *Nat. Commun.*, 2013, **4**, 2551.
74 E. C. Sañudo, W. Wernsdorfer, K. A. Abboud and G. Christou, *Inorg. Chem.*, 2004, **43**, 4137–4144.
75 A. J. Tasiopoulos, A. Vinslava, W. Wernsdorfer, K. a Abboud and G. Christou, *Angew. Chem. Int. Ed. Engl.*, 2004, **43**, 2117–2121.
76 J. Echeverría, G. Aullón, D. Danovich, S. Shaik and S. Alvarez, *Nat. Chem.*, 2011, **3**, 323–330.
77 J. Park, K. An, Y. Hwang, J. Park, H. Noh, J. Kim, J. Park, N. Hwang and T. Hyeon, *Nat. Mater.*, 2004, **3**, 891–895.
78 A. Saywell, G. Magnano, C. J. Satterley, L. M. a Perdigão, A. J. Britton, N. Taleb, M. del Carmen Giménez-López, N. R. Champness, J. N. O'Shea and P. H. Beton, *Nat. Commun.*,

2010, **1**, 75.
79 E. Fernandez-Bartolome, J. Santos, A. Gamonal, S. Khodabakhshi, L. J. McCornick, S. J. Teat, E. C. Sañudo, J. Sanchez Costa and N. Martin, *Angew. Chemie Int. Ed.*, , DOI:10.1002/anie.201812419.
80 J. R. Friedman, M. P. Sarachik, R. Ziolo and J. Tejada, *Phys. Rev. Lett.*, 1996, **76**, 3830–3833.
81 S. M. Suturin, V. V Fedorov, a G. Banshchikov, D. a Baranov, K. V Koshmak, P. Torelli, J. Fujii, G. Panaccione, K. Amemiya, M. Sakamaki, T. Nakamura, M. Tabuchi, L. Pasquali and N. S. Sokolov, *J. Phys. Condens. Matter*, 2013, **25**, 046002.
82 W. Wernsdorfer, N. Aliaga-Alcalde, D. N. Hendrickson and G. Christou, *Nature*, 2002, **416**, 406–9.
83 T. N. Nguyen, W. Wernsdorfer, K. a Abboud and G. Christou, *J. Am. Chem. Soc.*, 2011, **133**, 20688–20691.
84 C. Nistor, C. Krull, A. Mugarza, S. Stepanow, C. Stamm, M. Soares, S. Klyatskaya, M. Ruben and P. Gambardella, *Phys. Rev. B*, 2015, **92**, 184402.
85 C. T. Chen, Y. U. Idzerda, H. J. Lin, G. Meigs, A. Chaiken, G. A. Prinz and G. H. Ho, *Phys. Rev. B*, 1993, **48**, 642–645.
86 M. Gruber, F. Ibrahim, S. Boukari, H. Isshiki, L. Joly, M. Peter, M. Studniarek, V. Da Costa, H. Jabbar, V. Davesne, U. Halisdemir, J. Chen, J. Arabski, E. Otero, F. Choueikani, K. Chen, P. Ohresser, W. Wulfhekel, F. Scheurer, W. Weber, M. Alouani, E. Beaurepaire and M. Bowen, *Nat. Mater.*, 2015, **14**, 981–4.
87 G. Hadjipanayis, D. J. Sellmyer and B. Brandt, *Phys. Rev. B*, 1981, **23**, 3349–3354.
88 F. Magnus, M. E. Brooks-Bartlett, R. Moubah, R. A. Procter, G. Andersson, T. P. A. Hase, S. T. Banks and B. Hjörvarsson, *Nat. Commun.*, 2016, **7**, 1–7.